Pergamon

Int. J. Solids Structures Vol. 34, No. 13, pp. 1645–1665, 1997

0020–7683/97 $17.00 + .00

PII: S0020–7683(96)00053–4

INTERFACIAL CRACKING FROM THE FREE-EDGE OF A LONG BI-MATERIAL STRIP

A. R. AKISANYA
Aberdeen University Engineering Department, King's College, Aberdeen AB24 3UE, U.K.

and

N. A. FLECK
Cambridge University Engineering Department, Trumpington Street, Cambridge CB2 1PZ, U.K.

(*Received* 8 *August* 1995; *in revised form* 10 *April* 1996)

Abstract—A singular stress field develops at the corner where an interface between two bonded materials intersects a traction-free edge. Depending upon the geometry of the interface-corner, the free-edge stress singularity may be of the form $Hr^{\lambda-1}$, where r is the radial distance from the corner, $\lambda-1$ is the order of the stress singularity and H is the intensity of the singularity. The intensity H of the singularity developed at the free-edge of a long bi-material strip subjected to uniform tension is evaluated for various combinations of materials, using the finite element method. The role of the intensity H in controlling the initial growth of an interfacial edge crack embedded within the singularity zone is examined. The implications of the results for the initiation of free-edge cracks are discussed. © 1997 Elsevier Science Ltd. All rights reserved.

1. INTRODUCTION

The initiation and growth of cracks at the interface between two different elastic materials constitute major technical problems in the design of many multi-material systems, for example in the design of adhesive joints, thin film coatings and of composites. Failure of these multi-layer systems often initiates at the corner where the interface intersects a traction-free edge. The analysis of free-edge stress fields is therefore fundamental to our understanding of the initiation and growth of free-edge cracks.

The geometrical configuration at the edge of two bonded dissimilar materials is characterised by the angles θ_1 and θ_2 which the traction-free surfaces of the elastic materials make with the interface, as shown in Fig. 1. For this configuration, a displacement singularity of strength Hr^{λ} (and a corresponding stress singularity of type $Hr^{\lambda-1}$) can exist at the interface-corner; here, r is the radial distance from the corner, H is the intensity of the singularity and $\lambda-1$ is the order of the stress singularity. (We shall refer to this as the H-field, in contrast with a crack tip K-field.) The H-singularity occurs only within a local region near the interface-corner of the bi-material, and is therefore referred to as a free-edge effect. The value of λ may be real or complex, depending upon the relative elastic properties of the materials and upon the edge geometry (θ_1 and θ_2). However, the intensity, H, of the singularity depends upon the overall geometry of the strip, the material elastic properties and upon the remote loading. The value of H characterises the intensity of the stress state at the interface-corner.

An accurate determination of the order ($\lambda-1$) and the intensity, H, of the free-edge singularity is of paramount importance in predicting the local stress state at a free-edge. These stresses encourage the initiation and growth of free-edge cracks. Several studies have considered the evaluation of the order of the stress singularity $\lambda-1$, for different edge geometries and different combinations of materials (see, for example, Williams (1952), Bogy (1971), Hein and Erdogan (1971), Theocaris (1974), and van Vroonhoven (1992)). However, the evaluation of the intensity of the singularity, H, has received little attention. Reedy (1990, 1993) has determined the magnitude of H for (i) a thin elastic layer bonded

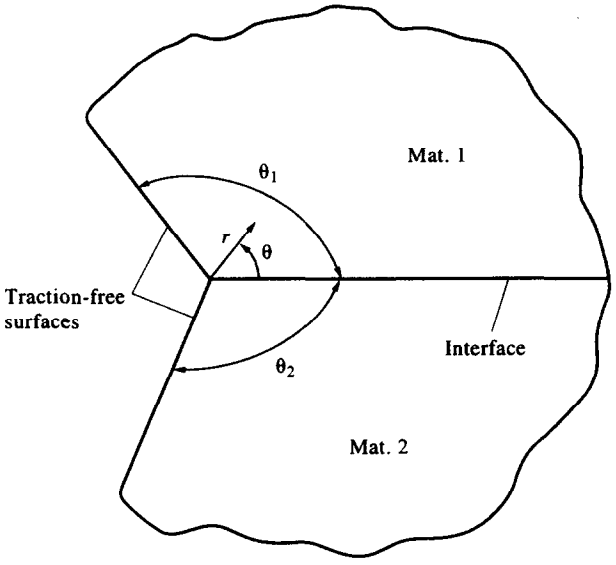

Fig. 1. General configuration at the free-edge of two bonded dissimilar materials.

to a rigid adherend, and (ii) for a thin elastic layer sandwiched between two rigid substrates. Several recent experimental studies have proposed the use of H to predict the failure of bonded materials in a manner similar to the use of conventional stress intensity factor for predicting the onset of crack growth (Gradin, 1982; Groth, 1988; Hattori *et al.*, 1989). A detailed calibration of the intensity of the free edge singularity H for different specimen geometries and material combinations is required for the effective application of an H-based failure criterion.

In this paper we calculate the intensity H of the singularity that occurs at the interface-corner A of a butt joint between two dissimilar but isotropic elastic strips, as shown in Fig. 2a. The length L of each strip is assumed to be much greater than the width w, and the remote ends are subjected to uniform tension σ. In addition we evaluate the interfacial stress intensity factor for an edge crack of length ℓ ($0 \leqslant \ell/w \leqslant 0.5$) at the interface between the two materials; see Fig. 2b. Some implications of the results for the initial growth of a free-edge crack within the singularity zone are discussed.

2. FORMULATION OF THE PROBLEM

2.1. *The bi-material geometry*

Consider the bi-material geometry shown in Fig. 2a. It consists of two elastic, isotropic and homogeneous strips bonded together to form a strip of width w and length $2L$, where $L \gg w$ (we take $L = 20w$). The strip is subjected to a remote tensile stress σ, and the strips are taken to be sufficiently thick for plane strain conditions to prevail. The material above the interface is termed material 1 while the material below the interface is termed material 2. For the geometry shown in Fig. 2a, the two materials are perfectly bonded along the interface (i.e., no interfacial crack is present). The traction-free sides of each strip makes an angle of $\pi/2$ with the interface at the interface-corner A, i.e., $\theta_1 = \theta_2 = \pi/2$. The stress field within a local region around the interface-corner A has a singularity of the form $Hr^{\lambda-1}$, where r is the distance from A and $\lambda - 1$ is the order of the stress singularity.

The geometry of the bi-material strip with an edge crack along the interface is shown in Fig. 2b. It is supposed that a crack has initiated at the corner A and exists as an interfacial crack of length ℓ, subjected to a remote tensile stress σ; see Fig. 2b. The interfacial stress intensity factor K (written in complex form as $K_1 + iK_2$, where $i = \sqrt{-1}$), and the non-singular stress terms parallel to the crack surface (referred to as the "T-stresses") are evaluated as functions of the relative crack length ℓ/w and elastic mismatch by the finite element method.

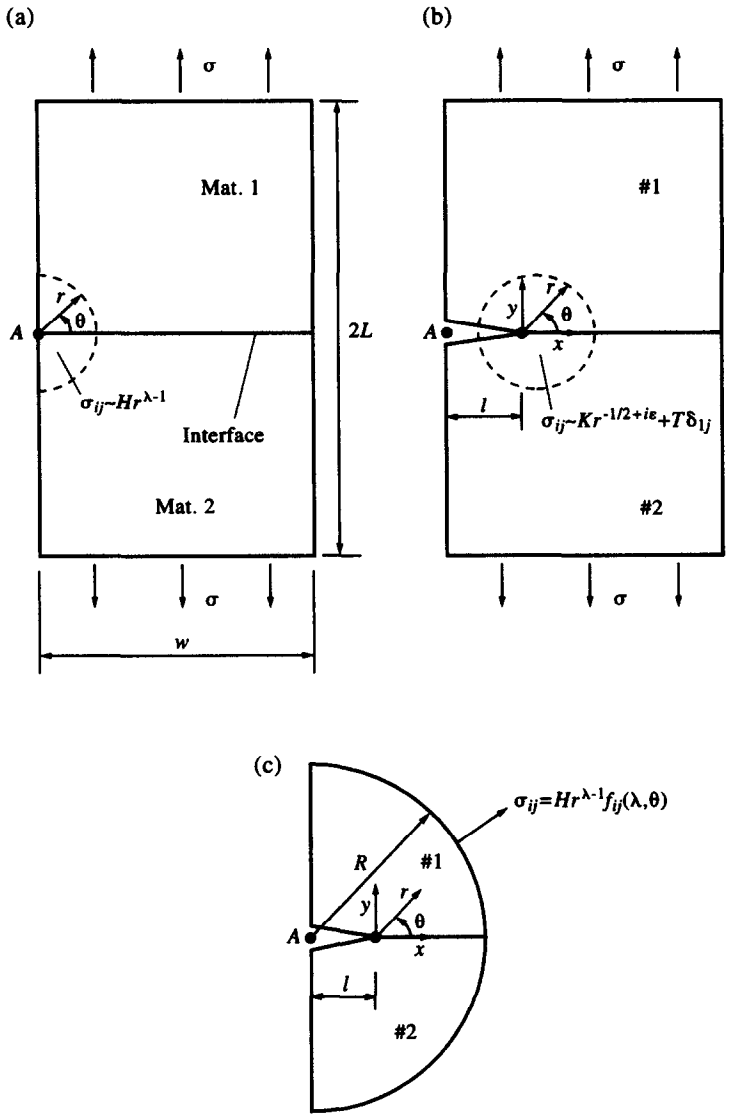

Fig. 2. The bi-material geometries. (a) An uncracked bi-material strip with perfect adhesion between the two materials. (b) A bi-material strip with an interfacial edge crack of length ℓ. (c) A boundary layer geometry for a short interfacial edge crack embedded within a free-edge singular field.

For the limiting case of small ℓ/w, the interfacial crack lies within the free-edge singularity characterised by H, and the interfacial K value is calculated in two steps as follows. First, the intensity H for the singular field is evaluated for the uncracked strip of finite width (Fig. 2a) via a contour integral and the finite element method. Second, the stress intensity factor for the short interfacial crack lying within the H-field is extracted by solving an ancillary boundary layer problem which couples the inner K-field with the outer H-field. The boundary layer problem is solved by the finite element method and makes use of the geometry shown in Fig. 2c. The external semi-circular boundary of the domain is loaded by the H-field, and the interfacial stress intensity factor for the embedded crack is extracted using a J-integral evaluation.

2.2. *Material elastic parameters*

Consider a bi-material consisting of two isotropic elastic materials loaded by prescribed surface tractions in plane strain or plane stress; Dundurs (1969) has shown that the stress distribution in such a body depends on only two combinations of the elastic constants. The two elastic mismatch parameters are defined for plane strain by

$$\alpha = \frac{\mu_1(\kappa_2+1)-(\kappa_1+1)\mu_2}{\mu_1(\kappa_2+1)+(\kappa_1+1)\mu_2} \tag{1a}$$

$$\beta = \frac{\mu_1(\kappa_2-1)-(\kappa_1-1)\mu_2}{\mu_1(\kappa_2+1)+(\kappa_1+1)\mu_2} \tag{1b}$$

where the subscripts refer to material 1 or 2, $\mu_j(=E_j/2(1+\upsilon_j))$, E_j, and υ_j denote shear modulus, Young's modulus and Poisson's ratio for material j, respectively, and $\kappa_j = 3-4\upsilon_j$ for plane strain. The material parameter α is positive when material 2 is more compliant than material 1, and is negative when material 2 is stiffer than material 1. Both α and β vanish when the elastic properties of both materials are identical, and switching materials 1 and 2 reverses the signs of α and β. The (α, β) values for typical material combinations are concentrated along $\beta = 0$ and $\beta = \alpha/4$ lines in $\alpha-\beta$ space (Suga *et al.*, 1988). In the current paper, we restrict our discussion to material combinations with $\beta = 0$ and $\beta = \alpha/4$.

2.3. *Intensity* H *of the free-edge singularity*

Let (r, θ) be cylindrical polar co-ordinates centred at the interface-corner A, as shown in Fig. 2a. By using a complex variable formulation, it is shown in Appendix A that the singular fields near the interface-corner are of the form

$$\sigma_{ij}^k = Hr^{\lambda-1} f_{ij}^k(\lambda, \theta)$$
$$u_i^k = Hr^{\lambda} g_i^k(\lambda, \theta) \tag{2}$$

where $(i,j) \equiv (r, \theta)$, $k(=1,2)$ is the material index, and f_{ij}^k and g_i^k are known functions of λ, θ and of the material mismatch parameters (α, β); explicit expressions for f_{ij}^k and g_i^k are given in Appendix A. We wish to evaluate H as a function of material elastic parameters (α, β) and of remote loading σ for the geometry shown in Fig. 2a. The order of the singularity λ has been determined for various corner geometries and material combinations: see, for example, Bogy (1971) and Hein and Erdogan (1971). The values of λ for the geometry shown in Fig. 2a are plotted in Fig. A1 of Appendix A, as a function of material elastic mismatch parameters α and β. When the two materials are identical ($\alpha = \beta = 0$) the singularity vanishes at the interface-corner and $\lambda = 1$ (Bogy, 1971; Kelly *et al.*, 1992). We note also that $\lambda(\alpha, \beta) = \lambda(-\alpha, -\beta)$.

The intensity H of the free-edge singularity will hereafter be referred to as the free-edge intensity factor. H is normalised with respect to the asymptotic singular field such that at a distance r from the interface-corner and along the interface ($\theta = 0$), the stress component normal to the interface, $\sigma_{\theta\theta}$, in the region dominated by the singularity is given by

$$\sigma_{\theta\theta}^1 = \sigma_{\theta\theta}^2 = Hr^{\lambda-1} \tag{3}$$

where the superscripts 1 and 2 denote the two materials. The free-edge intensity factor H depends, in general, upon the free-edge geometry, elastic mismatch parameters and upon the remote loading. Dimensional considerations dictate that H is related to the geometry and material elastic properties by

$$H = \sigma w^{1-\lambda} a(\alpha, \beta) \tag{4}$$

where σ is the remote stress, w is the width of the strip and a is a dimensionless function of the elastic parameters α and β. We shall evaluate $a(\alpha, \beta)$, and hence H, by a contour integral method and the finite element method, as described in Section 3.

2.4. *Stress intensities and T-stresses for an interfacial edge crack*

In general, an interfacial crack between two dissimilar isotropic elastic solids suffers a singular stress field characterised by the complex interfacial stress intensity factor $K = K_1 + iK_2$, where $i = \sqrt{-1}$. In order to define K we introduce the Cartesian co-ordinates

(x, y) and cylindrical polar co-ordinates (r, θ) placed at the crack tip as shown in Fig. 2b. Then, K is defined such that at a distance r directly ahead of the crack tip, the normal stress σ_{yy} and shear stress σ_{xy} are given by

$$\sigma_{yy}+i\sigma_{xy} = \frac{1}{\sqrt{2\pi}} K r^{-1/2+i\varepsilon} \tag{5}$$

where the oscillatory index ε depends only upon the material elastic mismatch parameter β via

$$\varepsilon = \frac{1}{2\pi}\ln\left(\frac{1-\beta}{1+\beta}\right). \tag{6}$$

It is clear from (5) that for $\varepsilon \neq 0$ the stress components oscillate as the crack tip is approached. This complicates the usual definition of mode mix at the crack tip. An approach suggested by Rice (1988) is to define the mode mix on the basis of the ratio σ_{xy}/σ_{yy} at a fixed distance $\hat{\ell}$ ahead of the crack tip. Accordingly, the phase angle $\hat{\psi}$ is introduced where

$$\tan\hat{\psi} = \left(\frac{\sigma_{xy}}{\sigma_{yy}}\right)_{r=\hat{\ell}} = \frac{\mathrm{Im}(K\hat{\ell}^{i\varepsilon})}{\mathrm{Re}(K\hat{\ell}^{i\varepsilon})}. \tag{7}$$

For a homogeneous solid where ($\alpha = \beta = 0$), K_1 and K_2 can be interpreted as the classical mode I and II stress intensity factors. As discussed by Rice (1988), the particular value taken for $\hat{\ell}$ usually has a negligible effect on the value of the phase angle $\hat{\psi}$ for realistic values of ε. Indeed for the case $\beta = \varepsilon = 0$, the phase angle $\hat{\psi}$ is independent of the particular choice of $\hat{\ell}$. In presenting the interfacial stress intensity solutions for both long and short edge cracks, it is convenient to define a phase angle ψ in relation to the crack length ℓ by

$$\tan\psi = \frac{\mathrm{Im}(K\ell^{i\varepsilon})}{\mathrm{Re}(K\ell^{i\varepsilon})}. \tag{8}$$

Note that ψ is related to $\hat{\psi}$ by

$$\psi = \hat{\psi} + \varepsilon\ln\left(\frac{\ell}{\hat{\ell}}\right). \tag{9}$$

In the series expansion for the interfacial crack tip stress field, the next highest order term to the K field is given by in-plane direct stresses parallel to the crack plane. These stresses are of magnitude T_1 in material 1 and T_2 in material 2, and are referred to as the 'T-stresses'. Since the strain component ε_{xx} is the same on both sides of the interface, a direct relation exists between the T-stresses,

$$T_2 = \frac{1-\alpha}{1+\alpha} T_1. \tag{10}$$

When the cracked bi-material strip shown in Fig. 2b is loaded by a remote tensile stress σ, the stress field at the tip of the interfacial crack of length ℓ from the free-edge is governed by the complex stress intensity factor K and the T-stresses T_1 in material 1 and T_2 in material 2. Dimensional considerations require that the stress intensity factor and the T-stresses be related to the geometry and the applied stress σ by

$$K\ell^{w} = \sigma\sqrt{\ell}\, b(\ell/w, \alpha, \beta) \tag{11}$$

$$T_1 = \sigma c(\ell/w, \alpha, \beta). \tag{12}$$

Here, $b(=b_1+ib_2)$ is a complex non-dimensional function and c a real non-dimensional function of the elastic mismatch parameters (α, β), and of the relative crack length ℓ/w. The T-stress T_2 in material 2 is related to the T-stress T_1 in material 1 via (10). The evaluation of these functions using the finite element method is described in Section 3.

For the case when the interfacial edge crack of length ℓ lies within the H-dominance zone the stress intensity factor and the T-stresses depend directly upon the magnitude of H. A boundary layer approach is used for evaluating the coupling between the crack tip parameters K and T and the free-edge singularity parameter H. The boundary layer geometry shown in Fig. 2c is loaded on the semi-circular boundary by the asymptotic free-edge displacement field characterised by H (eqn (2)).

The interfacial stress intensity factor K has the dimension (stress)(length)$^{1/2-i\varepsilon}$, while the free-edge intensity factor H has the dimension (stress)(length)$^{1-\lambda}$. Dimensional considerations require that the interfacial stress intensity factor K and the T-stress T_1 in material 1 be related to the geometry and the free-edge intensity factor H by

$$K\ell^{w} = H\ell^{\lambda-1/2} d(\alpha, \beta) \tag{13}$$

$$T_1 = H\ell^{\lambda-1} e(\alpha, \beta). \tag{14}$$

Here $d(=d_1+id_2)$ is a complex non-dimensional function and e a real non-dimensional function of the elastic mismatch parameters α and β; the evaluation of these functions is described in Section 3.

By substituting the expression (4) for the free-edge intensity factor H into (13) and (14), the interfacial stress intensity factor K and the T-stress T_1 in material 1 for an interfacial crack embedded within the free-edge singularity zone are given in terms of the remote loading σ, crack length ratio ℓ/w and of the material parameters (α, β) by

$$K\ell^{w} = \sigma\sqrt{\ell}\left(\frac{\ell}{w}\right)^{\lambda-1} a(\alpha, \beta) \cdot d(\alpha, \beta) \tag{15}$$

$$T_1 = \sigma\left(\frac{\ell}{w}\right)^{\lambda-1} a(\alpha, \beta) \cdot e(\alpha, \beta). \tag{16}$$

The order of the stress singularity $(\lambda-1)$ is also a function of α and β. Recall that a and e are real, and d is a complex non-dimensional function.

3. NUMERICAL ANALYSIS

The finite element method is used to evaluate the free-edge intensity factor H for the uncracked bi-material strip (Fig. 2a), and the interfacial stress intensity factor K and the T-stress T_1 in material 1, for the cracked strip (Figs 2b and 2c). Numerical computations were performed for a bi-material strip having a length of $2L = 20w$, where w is the width of the strip, and the strip is subjected to a uniform remote tensile stress σ. Results are obtained for various values of material parameters α and β $(=0$ and $\alpha/4)$, and for values of relative crack length ℓ/w in the range $0.06 \leqslant \ell/w \leqslant 0.5$. First we describe the procedure for the evaluation of the free-edge intensity factor H.

3.1. *Evaluation of the free-edge intensity factor* H

The free-edge intensity factor H is determined by the 'reciprocal work integral contour method'. The method involves a convolution of the asymptotic field of the corner singularity

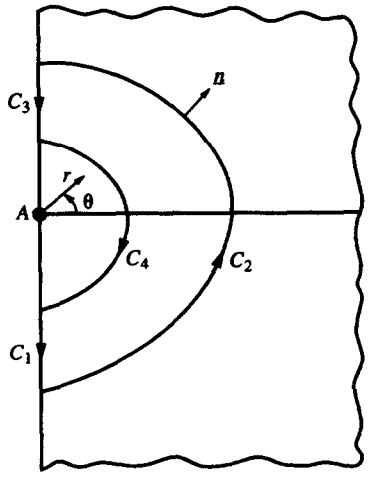

Fig. 3. A closed integration path around the interface-corner A.

with a finite element solution. This contour integral method has been used by various authors to obtain the stress intensities for different crack and notch geometries; see, for example, Stern *et al.* (1976), Sinclair *et al.* (1985), and Carpenter and Byers (1987). The method is based on Betti's reciprocal law (Sokolnikoff, 1956), and is outlined below.

Consider a closed contour $C(=C_1+C_2+C_3+C_4)$ around the interface-corner A, as shown in Fig. 3. Betti's reciprocal law can be stated as

$$\oint_C (\sigma_{ij}u_i^* - \sigma_{ij}^* u_i) n_j \, ds = 0 \tag{17}$$

where $(i,j) \equiv (r,\theta)$ represent polar co-ordinates centred at the interface-corner, σ_{ij} and u_i are the free-edge singular stress and displacement fields given by eqn (2), σ_{ij}^*, u_i^* are auxiliary fields satisfying the same boundary conditions as σ_{ij} and u_i, n_j is the outward unit normal to C, and ds is an infinitesimal line segment of C. Integration in (17) is performed in an anticlockwise sense around C. By appropriate choice of the auxiliary field (σ_{ij}^*, u_i^*), the integral (17) can be used to determine the free-edge intensity factor H.

In the evaluation of H the auxiliary fields σ_{ij}^* and u_i^* are chosen as the free-edge singular stress and displacement fields given by (2) with intensity H^* and λ replaced by $\lambda^* = -\lambda$. The starred fields (σ_{ij}^*, u_i^*) with $\lambda^* = -\lambda$ satisfy the same boundary conditions as those for the unstarred fields (σ_{ij}, u_i). These boundary conditions are: (1) traction-free conditions along $\theta = -\pi/2$ and $\theta = \pi/2$, and (ii) continuity of displacements and stress components $(\sigma_{\theta\theta}, \sigma_{r\theta})$ along the interface, where (r,θ) are polar coordinates centred at the interface-corner; see Fig. 2a. The unstarred fields (σ_{ij}, u_i) are obtained for the bi-material strip geometry of Fig. 2a using the finite element method. The value of the intensity H^* for the auxiliary field is chosen such that the evaluation of (17) by the domain integration method gives the intensity H for the elastic state of interest. A more detailed description of the procedure for the evaluation of H is given in Appendix B. Once the value of H has been obtained, we calculate the non-dimensional constant $a(\alpha,\beta)$ via eqn (4).

Elastic analysis of the uncracked bi-material strip of Fig. 2a has been carried out using the finite element code ABAQUS†. The finite element mesh consists of 586 eight-noded plane strain isoparametric, quadrilateral elements. The mesh near the interface-corner is refined due to the presence of the singularity; a typical finite element mesh is given in Fig. 4a. The width of the strip w is taken as unity and the strip length $2L = 20w$. Only one half of the width of the uncracked bi-material strip is analysed due to symmetry: roller boundary conditions are applied along the mid-plane of the strip. The results for the coefficient a are listed in Table 1 for various values of material parameters α and β ($=0$ and $\alpha/4$).

† Hibbitt, Karlsson and Sorenson, ABAQUS Users Manual, Version 5.2, HKS Inc. (1992).

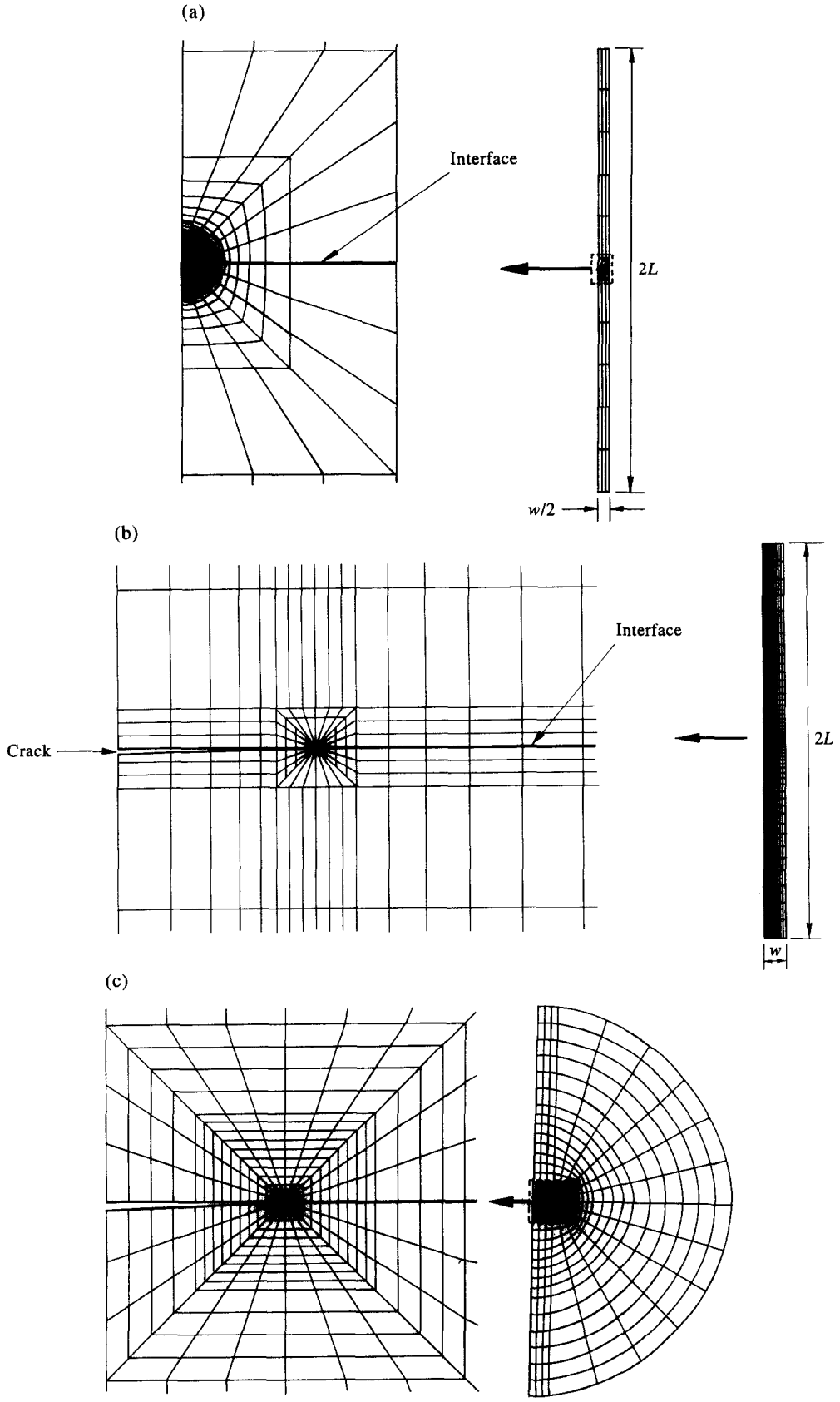

Fig. 4. The finite element meshes. (a) Uncracked bi-material strip, $L = 10w$. (b) Bi-material strip with an interfacial edge crack, $L = 10w$. (c) Boundary layer geometry; the crack length $\ell = R/100$, where R is the outer radius of the boundary layer.

Tables 1–5. Tabulated solutions of the non-dimensional constants a, $b(=b_1+ib_2)$, c, $d(=d_1+id_2)$ and e as functions of material elastic mismatch parameters α and $\beta(=0$ and $\alpha/4)$.

Table 1. $a(\alpha, \beta)$

	$\alpha = 0$	$\alpha = 0.2$	$\alpha = 0.5$	$\alpha = 0.8$	$\alpha = 0.99$
$\beta = 0$	0.99998	0.89536	0.63182	0.43335	0.33653
$\beta = \alpha/4$	0.99998	0.94761	0.75395	0.54718	0.42792

Note that $a(-\alpha, -\beta) = a(\alpha, \beta)$.

Table 2. $b = b_1+ib_2$

		$\alpha = 0$	$\alpha = 0.2$		$\alpha = 0.5$		$\alpha = 0.8$		$\alpha = 0.99$	
ℓ/w		$\beta = 0$	$\beta = 0$	$\beta = \alpha/4$	$\beta = 0$	$\beta = \alpha/4$	$\beta = 0$	$\beta = \alpha/4$	$\beta = 0$	$\beta = \alpha/4$
0.06	b_1	2.0096	2.0408	2.0268	2.2001	2.1211	2.5057	2.3192	2.7057	2.5232
	b_2	−0.0001	−0.1813	−0.1460	−0.4662	−0.3835	−0.8086	−0.6747	−1.1570	−0.9141
0.08	b_1	2.0516	2.0749	2.0652	2.1933	2.1399	2.4175	2.2958	2.5774	2.4547
	b_2	−0.0001	−0.1701	−0.1317	−0.4332	−0.3429	−0.7401	−0.5939	−1.0197	−0.7923
0.10	b_1	2.0967	2.1145	2.1079	2.2063	2.1699	2.3770	2.2986	2.5075	2.4290
	b_2	−0.0001	−0.1614	−0.1208	−0.4077	−0.3127	−0.6878	−0.5358	−0.9514	−0.7073
0.20	b_1	2.4150	2.4220	2.4219	2.4564	2.4598	2.5169	2.5359	2.5967	2.6098
	b_2	−0.0001	−0.1302	−0.0872	−0.3242	−0.2231	−0.5343	−0.3733	−0.6694	−0.4822
0.30	b_1	2.9314	2.9347	2.9376	2.9495	2.9711	2.9677	3.0366	3.0281	3.0978
	b_2	−0.0001	−0.1038	−0.0661	−0.2580	−0.1679	−0.4264	−0.2777	−0.5899	−0.3548
0.40	b_1	3.7287	3.7296	3.7352	3.7311	3.7702	3.7213	3.8366	3.7235	3.8935
	b_2	−0.0001	−0.0742	−0.0483	−0.1846	−0.1215	−0.3092	−0.1970	−0.4348	−0.2474
0.50	b_1	4.9869	4.9853	4.9949	4.9719	5.0351	4.9281	5.1099	4.9981	5.1783
	b_2	−0.0001	−0.0350	−0.0312	−0.0885	−0.0763	−0.1555	−0.1171	−0.1513	−0.1392

Note that $b_1(-\alpha, -\beta) = b_1(\alpha, \beta)$ and $b_2(-\alpha, -\beta) = -b_2(\alpha, \beta)$.

3.2. *Evaluation of the interfacial stress intensity factor and* T-*stresses*

Both the interfacial stress intensity factor K and the T-stresses are determined by (i) evaluating the path-independent J-integral for the elastic state of interest, followed by (ii) evaluating the J-integral for a linear superposition of the elastic state of interest and a suitably chosen auxiliary elastic field.

Parks' (1974) virtual crack extension method is used to evaluate the path independent J-integral. For the evaluation of the components K_1 and K_2 of the interfacial stress intensity factor, the auxiliary field is taken to be the singular crack tip field for an interfacial crack, as described by Matos *et al.* (1989). In the evaluation of the T-stresses, the auxiliary elastic field consist of a point force placed at the tip of the semi-infinite interfacial crack and in a direction parallel to the crack faces. A detailed description of these methods is given by Akisanya and Fleck (1994).

Finite element analysis is carried out using the finite element code ABAQUS. The finite element mesh contains 1236 to 1516 elements for the case of long crack (Figs 2b and 4b) and 638 elements for the boundary layer problem (Figs 2c and 4c). In all cases eight-noded plane strain isoparametric, quadrilateral elements are used.

The numerically obtained values for the coefficients b, c, d and e are listed in Tables 2–5, for various values of material parameters α and β $(=0$ and $\alpha/4)$, and relative crack length in the range $0.06 \leqslant \ell/w \leqslant 0.5$. The results are compared with existing solutions (Sham, 1991) for the coefficients b and c when the two materials are identical (i.e., $\alpha = \beta = 0$) and $\ell/w \geqslant 0.1$: we find that our results are accurate to within about 1%.

4. RESULTS

4.1. *Zone of dominance of the free-edge singularity*

The extent of the region dominated by the free-edge singularity is estimated by comparing the finite element solutions with the singular asymptotic solutions given by eqn (2).

Table 3. $c(\alpha, \beta)$

	$\alpha = 0$	$\alpha = 0.2$		$\alpha = 0.5$		$\alpha = 0.8$		$\alpha = 0.99$	
ℓ/w	$\beta = 0$	$\beta = 0$	$\beta = \alpha/4$	$\beta = 0$	$\beta = \alpha/4$	$\beta = 0$	$\beta = \alpha/4$	$\beta = 0$	$\beta = \alpha/4$
0.06	−0.5588	−0.6762	−0.6732	−0.8988	−0.8763	−1.1986	−1.1199	−1.5637	−1.3563
0.08	−0.5535	−0.6732	−0.6717	−0.8844	−0.8678	−1.1571	−1.0925	−1.4455	−1.3062
0.10	−0.5521	−0.6728	−0.6722	−0.8756	−0.8638	−1.1241	−1.0769	−1.3833	−1.2765
0.20	−0.6011	−0.7191	−0.7184	−0.9155	−0.9111	−1.1231	−1.1100	−1.2914	−1.2809
0.30	−0.6155	−0.7494	−0.7485	−0.9574	−0.9511	−1.1705	−1.1546	−1.3110	−1.3451
0.40	−0.5869	−0.7200	−0.7180	−0.9275	−0.9168	−1.1455	−1.1123	−1.0155	−1.3223
0.50	−0.4336	−0.5437	−0.5417	−0.7206	−0.7016	−0.9116	−0.8523	−0.4554	−1.0734

Note that $c(-\alpha, -\beta) = c(\alpha, \beta) \cdot (1-\alpha)/(1+\alpha)$.

Table 4. $d = d_1 + id_2$

	$\alpha = 0$		$\alpha = 0.2$		$\alpha = 0.5$		$\alpha = 0.8$		$\alpha = 0.99$	
	d_1	d_2	d_1	d_2	d_1	d_2	d_1	d_2	d_1	d_2
$\beta = 0$	1.9241	−0.0001	1.9611	−0.1831	2.0957	−0.4109	2.2639	−0.5991	2.2803	−0.6468
$\beta = \alpha/4$	1.9241	−0.0001	1.9426	−0.1404	2.0343	−0.3558	2.1911	−0.5620	2.3259	−0.6793

Note that $d_1(-\alpha, -\beta) = d_1(\alpha, \beta)$ and $d_2(-\alpha, -\beta) = -d_2(\alpha, \beta)$.

Table 5. $e(\alpha, \beta)$

	$\alpha = 0$	$\alpha = 0.2$	$\alpha = 0.5$	$\alpha = 0.8$	$\alpha = 0.99$
$\beta = 0$	−0.5109	−0.6150	−0.7532	−0.8852	−0.9741
$\beta = \alpha/4$	−0.5109	−0.6112	−0.7564	−0.8998	−0.9947

Note that $e(-\alpha, -\beta) = e(\alpha, \beta) \cdot (1-\alpha)/(1+\alpha)$.

The stress component $\sigma_{\theta\theta}$ along the radial direction $\theta = 43°$, and near the interface ($\theta = 1.6°$) is plotted against the radial distance from the interface-corner r in Fig. 5, for $\alpha = 0.5$ and $\alpha = 0.8$, and for $\beta = 0$ and $\beta = \alpha/4$. Here, (r, θ) are cylindrical polar co-ordinates centred at the interface-corner as shown in Fig. 2a. The stress component $\sigma_{\theta\theta}$ is normalised by the applied remote tension σ while the radial distance r is normalised by the strip width w. The asymptotic and finite element results for $\sigma_{\theta\theta}$ along $\theta = 43°$ are in good agreement for $r/w < 0.1$ and differ only by about 6% at $r/w = 0.25$ (see Fig. 5a). However, the asymptotic and the finite element solutions for $\sigma_{\theta\theta}$ along $\theta = 1.6°$ are only in agreement for $r/w < 0.03$. Thus, the free-edge singularity along a radial direction away from the interface (e.g., along $\theta \approx 43°$) dominates a significant fraction of the width of the bi-material strip considered. This observation is qualitatively similar to that of a thin elastic layer sandwiched between two rigid substrates where the free-edge singularity dominates a region of the order of 0.6 times the layer thickness (Reedy, 1993). The extent of the singular zone along the interface ($\theta \approx 0$) is in good agreement with that obtained by Bogy (1975) for an infinitely long bi-material strip of width w, elastic mismatch parameters $\alpha = -0.8$, $\beta = 0$, and subjected to a remote tension: the stress component $\sigma_{\theta\theta}$ along the interface is greater than the applied tension over the interval $0 < r/w < 0.05$, where r is the radial distance from the interface corner.

We find that the normalised stress component $\sigma_{\theta\theta}$ within the singularity zone is a maximum at the interface with a value which is dependent upon the material elastic properties. This suggests that crack initiation is more likely to occur at or near the interface. There is a significant effect of the material elastic parameter β on the magnitude of $\sigma_{\theta\theta}$ in the region dominated by the free edge singularity along both $\theta = 43°$ and $\theta = 1.6°$: for a given value of α, $\sigma_{\theta\theta}$ decreases with increasing β.

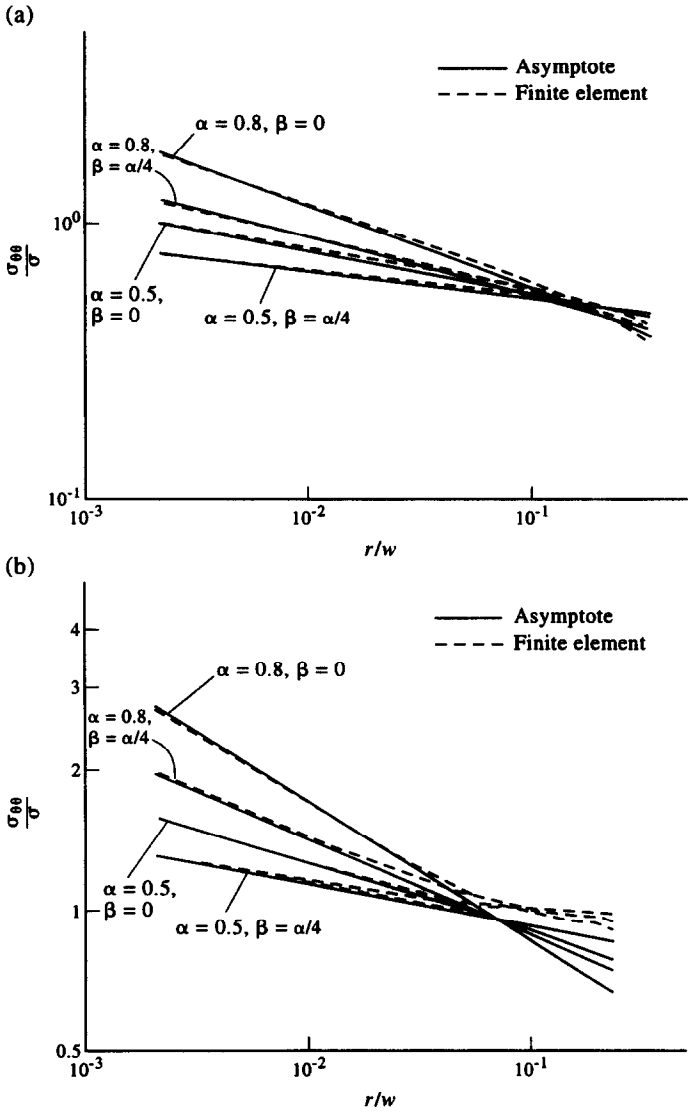

Fig. 5. Comparison of the linear elastic finite element and asymptotic singular solutions for stress component $\sigma_{\theta\theta}$ along (a) $\theta = 43°$, and (b) $\theta = 1.6°$.

4.2. *Magnitude of the free-edge intensity factor* H

The magnitude of the free-edge intensity factor H is related to the applied stress σ, the strip width w and the material elastic properties (α, β) in the manner given by eqn (4). The non-dimensional constants $a(\alpha, \beta)$ are determined by the contour integral method as described in Appendix A. Values for a are listed in Table 1 and are plotted in Fig. 6a, as a function of material parameters α and β ($=0$ and $\alpha/4$). The function a is almost symmetric about the $\alpha = 0$ line in Fig. 6a. It decreases from a value of unity in the homogeneous limit $\alpha = \beta = 0$ to a value of about 0.4 when $|\alpha| = 1$ and $|\beta| = 0$ and $\alpha/4$. We further note that a increases with increasing β. The shape of the a vs α curve plotted in Fig. 6b is qualitatively similar to that of the λ vs α plot shown in Fig. A1. A cross-plot of a vs λ is given in Fig. 6b: it reveals that the results for $\beta = 0$ and $\beta = \alpha/4$ collapse onto a single curve to within numerical accuracy. We conclude that a scales directly with λ for all (α, β) considered.

The intensity factor H is a useful measure of the *initiation strength* of a joint provided any region of inelasticity is embedded within the H-field. For any particular material system, the critical value of H (say H_{crit}) can be measured by experiments using the calibration (4). The use of an H-based failure criterion is justified provided the inelastic damage zone at the free-edge is contained within the asymptotic singular field. Consider, for example, the common case of a butt joint where two different elastic solids 1 and 2 are bonded together

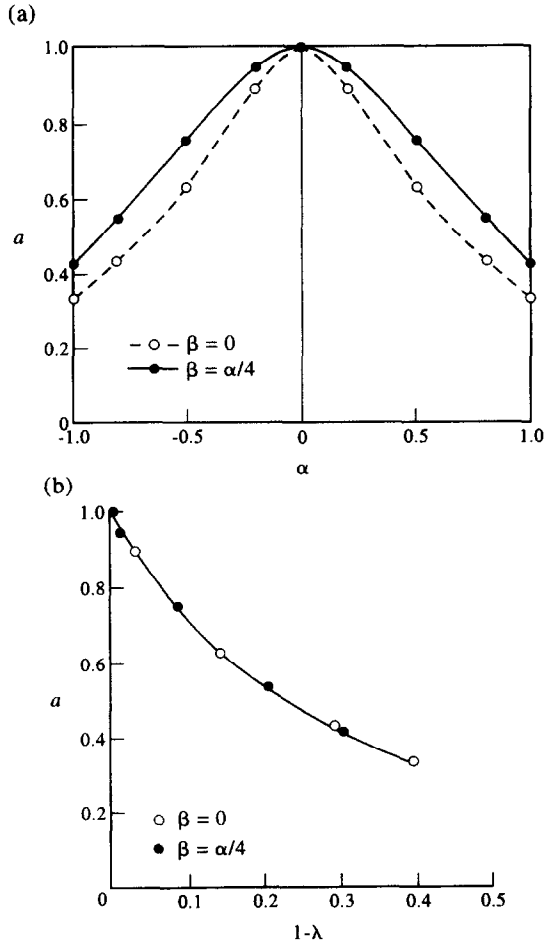

Fig. 6. The non-dimensional constant a as a function of (a) the material elastic mismatch parameters α and β, and (b) the order of the stress singularity $1-\lambda$.

by a thin layer of a third elastic solid (material 3). When the layer thickness is much less than the width w of the panel, the presence of the sandwich layer can be neglected in the definition of H, and H is defined on the basis of materials 1 and 2. The physical idea is that the sandwich layer finds itself embedded within an outer H-field associated with the adherends; provided failure occurs within the zone of H-dominance, the parameter H is a valid parameter for characterising the fracture strength of the structure.

4.3. *Interfacial stress intensity factor*

The non-dimensional real and imaginary components of the complex interfacial stress intensity factor defined by (11) and (13) are plotted in Figs 7 and 8, respectively. Recall that for the homogeneous case $K_1 = \mathrm{Re}(K\ell^{i\varepsilon}) = 1.12\sigma\sqrt{\pi\ell} = 1.985\sigma\sqrt{\ell}$ and $K_2 = \mathrm{Im}(K\ell^{i\varepsilon}) = 0$. Consequently, results for K in Figs 7 and 8 have been normalised by $\sigma\sqrt{\ell}$. The stress intensity factor values shown for ℓ/w in the interval $10^{-5} \leqslant \ell/w \leqslant 10^{-3}$ are the asymptotic results for a crack embedded within the free-edge singularity zone (see Fig. 2c); results for $\ell/w \geqslant 0.06$ correspond to a long interfacial crack (see Fig. 2b) and are determined by a finite element analysis of the cracked strip shown in Fig. 2b. The solutions of Sham (1991) for the homogeneous solid are included in Fig. 7a for comparison; the present results are accurate to within about 1%.

There is a significant β-effect on both the real and the imaginary components of the stress intensity factor in the region dominated by the singularity; the effect diminishes far away from the free-edge singularity zone. The real component of the stress intensity factor $\mathrm{Re}(K\ell^{i\varepsilon})$ is positive while the imaginary component $\mathrm{Im}(K\ell^{i\varepsilon})$ is negative for all combinations of materials considered. We note in passing that the real component $\mathrm{Re}(K\ell^{i\varepsilon})$ is symmetric

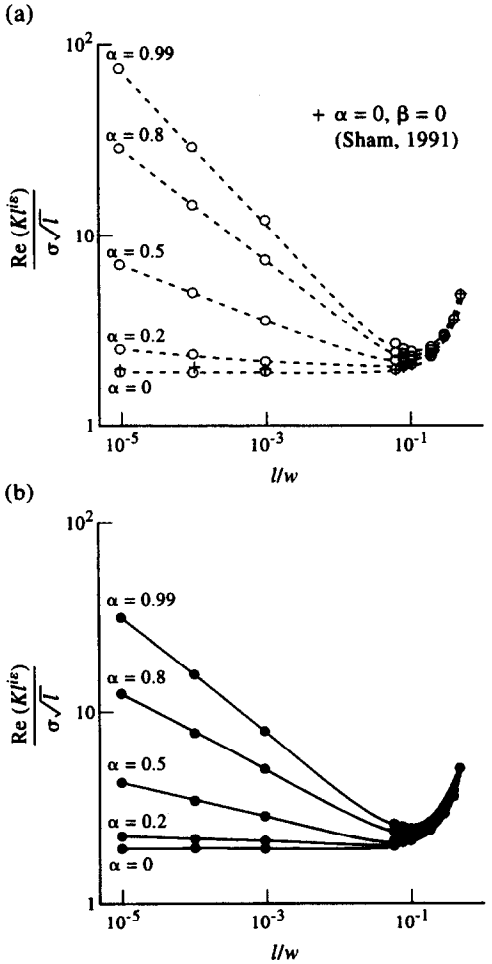

Fig. 7. The effect of elastic mismatch parameters (α, β) and relative crack length ℓ/w upon the real component of the interfacial stress intensity factor $\text{Re}(K\ell^{i\varepsilon})/\sigma\sqrt{\ell}$. (a) $\beta = 0$, and (b) $\beta = \alpha/4$.

while the imaginary component $\text{Im}(K\ell^{i\varepsilon})$ is anti-symmetric with respect to the sign of the material parameters (α, β).

It is evident from Figs 7 and 8 that the interfacial stress intensity factor for short crack lengths ($\ell/w < 0.1$) is significantly amplified by the presence of the free edge singularity. The magnitude of the normalised stress intensity factor decreases with increasing crack length within the singularity region: the effect of the singularity on the stress intensity factor diminishes as the crack length increases. In Fig. 7 the real component of the stress intensity factor $\text{Re}(K\ell^{i\varepsilon})$ collapses to almost a single curve for all (α, β) considered when the crack is sufficiently long ($\ell/w > 0.1$).

4.4. *The interfacial* T-*stress*

Figure 9 shows the normalised T-stress T_1/σ in material 1 (i.e., the material above the interface) due to remote tensile loading σ, as a function of relative crack length ℓ/w. The corresponding normalised T-stress T_2/σ in material 2 are obtained via eqn (10) from which it can be shown that $T_1(-\alpha, -\beta) = T_1(\alpha, \beta) \cdot (1-\alpha)/(1+\alpha)$. We observe that T_1 is negative for all material combinations considered. The magnitude of T_1 decreases with increasing crack length for a crack that lies with the singularity zone (Fig. 9); it remains fairly constant for a crack whose tip is outside the singularity zone, and decreases rapidly as the crack tip approaches the mid-plane of the bi-material strip (i.e., as $\ell/w \to 0.5$), see Fig. 9. There is a significant β-effect on the magnitude of T_1 for short edge cracks; the effect decreases with increasing crack length and with decreasing value of α. A comparison of the solutions for $\alpha = \beta = 0$ with those of Sham (1991) show that our results are accurate to within 0.5%.

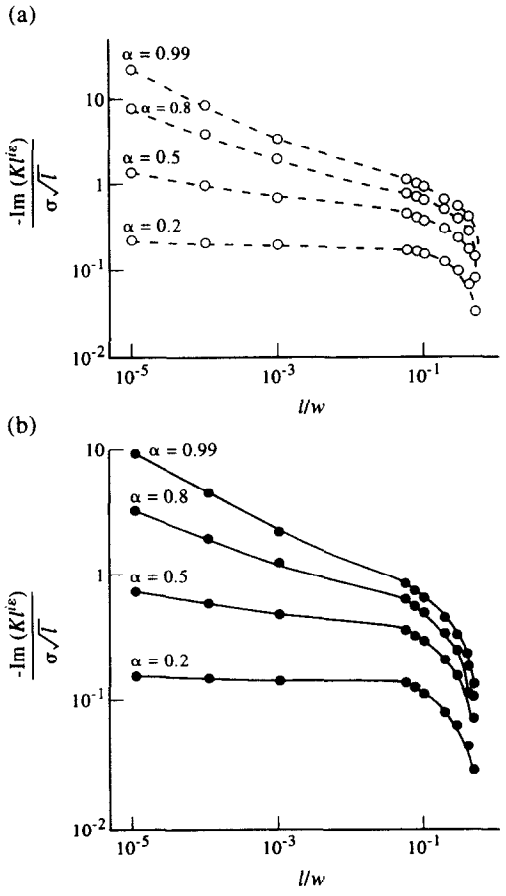

Fig. 8. The effect of elastic mismatch parameters (α, β) and relative crack length ℓ/w upon the imaginary component of the interfacial stress intensity factor $\mathrm{Im}(K\ell^{ie})/\sigma\sqrt{\ell}$. (a) $\beta = 0$, and (b) $\beta = \alpha/4$.

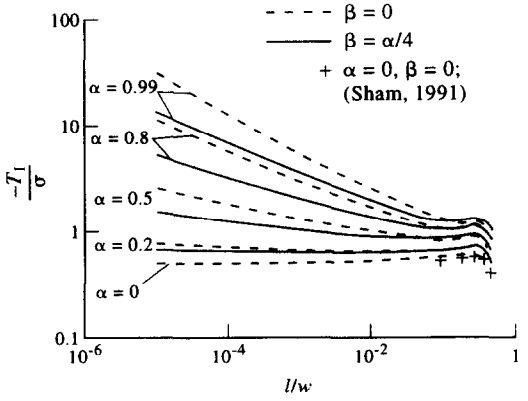

Fig. 9. The effect of elastic mismatch parameters (α, β) and relative crack length ℓ/w upon the T-stress in material 1, T_1.

The magnitude and sign of the T-stress affect kinking of an interfacial crack out of the interface (He *et al.*, 1991; Akisanya and Fleck, 1994). A positive value of T-stress both encourages kinking of an interfacial crack and causes the kinked crack to grow unstably under a fixed remote loading. In addition, the subsequent trajectory of the kink is expected to diverge from the interface if the T-stress is positive (Cotterell and Rice, 1980). A negative value of the T-stress has the following effects: (i) it stabilises an interfacial crack against

kinking, (ii) it may cause a kinked crack to arrest, and (iii) crack growth from an initial kink is expected to converge towards the interface.

4.5. *Strain energy release rate and phase angle*

The normalised strain energy release rate $E^*G_I/\sigma^2 w$ is given by

$$\frac{E^*G_I}{\sigma^2 w} = \left(\frac{\ell}{w}\right)^{2\lambda-1} a^2(d_1^2 + d_2^2) \tag{18a}$$

for a crack within the free-edge singularity zone, and by

$$\frac{E^*G_I}{\sigma^2 w} = \left(\frac{\ell}{w}\right)(b_1^2 + b_2^2) \tag{18b}$$

for a crack whose tip is outside the singularity region. Here, $E^* \equiv (1+\alpha)/(1-\beta^2)E_2/(1-\nu_2^2)$ where E_2 and ν_2 are the Young's modulus and the Poisson's ratio of material 2 below the interface. The corresponding phase angle of loading at the crack tip ψ defined by (8) is obtained by using eqns (13) or (15). Once the calibration functions $a(\alpha, \beta)$, $b(\ell/w, \alpha, \beta)$ and $d(\alpha, \beta)$ have been deduced from the finite element analysis, the quantities G_I and ψ are known for any prescribed remote loading σ and strip width w. Recall that the coefficient a is real, while coefficients b and d are complex functions; the values of these coefficients are given in Tables 1, 2 and 4, respectively.

Results for $E^*G_I/\sigma^2 w$ and ψ are given in Fig. 10. Interfacial toughness data are usually presented in the $G_I - \psi$ plane; it is therefore instructive to display our results by taking $E^*G_I/\sigma^2 w$ and ψ as axes in Fig. 10. Each curve is for a prescribed (α, β) value and is a trajectory of ℓ/w in the range 10^{-4} to 0.5. The dashed lines correspond to the solutions for a crack embedded within the singularity zone.

The normalised strain energy release rate $E^*G_I/\sigma^2 w$ increases monotonically from zero as the crack length is increased with little attendant change in the phase angle ψ. This suggests that interfacial crack growth from the free edge is unstable under fixed remote loading. The effect of the material elastic mismatch parameter β upon the values of $E^*G_I/\sigma^2 w$ and ψ is minor. Also, the effect of the material mismatch parameter α upon the magnitude of $E^*G_I/\sigma^2 w$ is small for $\ell/w \geqslant 0.1$.

5. CONCLUDING REMARKS

A singularity of the type $Hr^{\lambda-1}$ exists at the free-edge of a butt joint between two dissimilar elastic solids under remote tension. In this paper we have presented a finite element analysis for the evaluation of the intensity H and the order of the stress singularity $\lambda - 1$. The intensity H is evaluated by a contour integral method. The singular zone along a radial direction of $\theta \approx 45^\circ$ from the interface extends to a distance of about $0.1w$ from the interface-corner, where w is the width of the bi-material strip. However, the zone of dominance of the free-edge singularity near the interface ($\theta \approx 0$) is more localised, extending to a radial distance of about $r = 0.03w$ from the interface corner. It is expected that H provides a useful correlating parameter for fracture initiation at the free-edge of the butt-joint.

In the finite element evaluation of the free-edge intensity factor H for the uncracked bi-material strip we have taken the length L to equal $20w$, where w is the width of the strip. Numerical experimentation showed that this ratio of L/w is sufficiently large for the results to be independent of L: the numerical results pertain to the case of a long strip, with w as the only length-scale in the problem.

A calibration of the interfacial stress intensity factor K and the T-stress is given for a crack lying within the singularity region and also for a crack whose tip is outside the singularity zone. There is a significant effect of the H-singularity field on the magnitude of

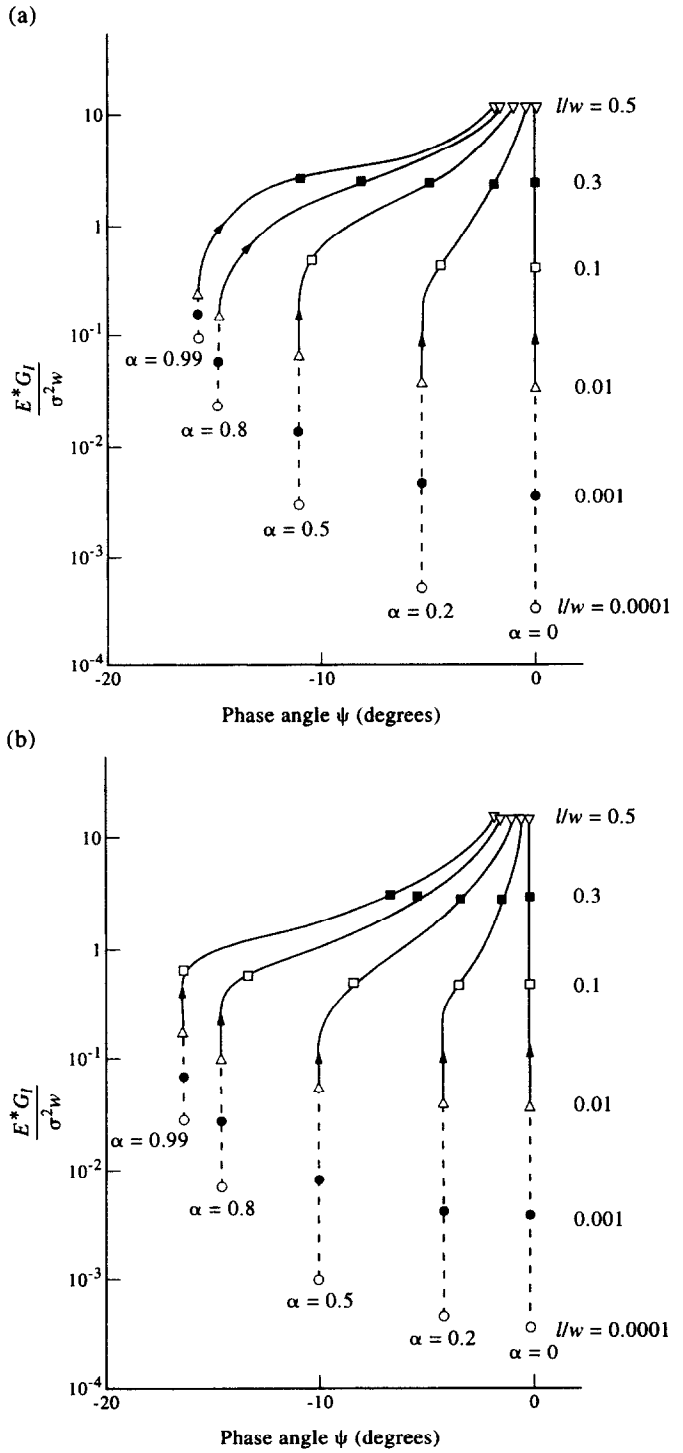

Fig. 10. The effect of elastic mismatch parameters (α, β) and relative crack length ℓ/w upon the non-dimensional energy release rate $E^*G_I/\sigma^2 w$ and the phase angle $\psi = \arctan[\mathrm{Im}(K\ell^{ie})/\mathrm{Re}(K\ell^{ie})]$. (a) $\beta = 0$, and (b) $\beta = \alpha/4$. The arrows indicate the direction of increasing relative crack length ℓ/w.

the stress intensity factor and upon the T-stress for the crack. The energy release rate for the interfacial edge crack increases monotonically with crack extension : the crack is unstable under fixed load.

Acknowledgements—The authors are grateful to Prof. J. W. Hutchinson for helpful discussions. Financial support is gratefully acknowledged from the Procurement Executive of the Ministry of Defence (contract 2029/267) and the Office of Naval Research (contract 0014-91-J-1916).

REFERENCES

Akisanya, A. R. and Fleck, N. A. (1994). The edge cracking and decohesion of thin films. *Int. J. Solids Struct.* **31,** 3175–3199.

Bogy, D. B. (1971). Two edge-bonded elastic wedges of different materials and wedge angles under surface tractions. *J. Appl. Mech.* **38,** 377–386.

Carpenter, W. C. and Byers, C. (1987). A path independent integral for computing stress intensities for V-notched cracks in bi-materials. *Int. J. Fract.* **35,** 245–268.

Cotterell, B. and Rice, J. R. (1980). Slightly curved or kinked cracks. *Int. J. Fract.* **16,** 155–169.

Dundurs, J. (1969) *Mathematical Theory of Dislocations*, American Society of Mech. Engineers, NY.

England, A. H. (1971). On stress singularities in linear elasticity. *Int. J. Engng Sci.* **9,** 571–585.

Gradin, P. A. (1982). A fracture criterion for edge-bonded bi-material bodies. *J. Comp. Mat.* **16,** 448–456.

Groth, H. L. (1988). Stress singularities and fracture at interface-corners in bonded joints. *Int. J. Adhesion Adhesives* **8,** 107–113.

Groth, H. L. and Brottare, I. (1988). Evaluation of singular intensity factors in elastic–plastic materials. *J. Testing Evaluation* **16,** 291–297.

Hattori, T., Sakata, S. and Murakami, G. (1989). A stress singularity parameter approach for evaluating the interfacial reliability of plastic encapsulated LSI devices. *J. Electronic Packaging* **111,** 243–248.

He, M. Y., Bartlett, A., Evans, A. G. and Hutchinson, J. W. (1991). Kinking of a crack out of an interface: role of in-plane stress. *J. Am. Ceram. Soc.* **74,** 767–771.

Hein, V. L. and Erdogan, F. (1971). Stress singularities in a two-material wedge. *Int. J. Fract. Mech.* **7,** 317–330.

Kelly, P. A., Hills, D. A. and Nowell, D. (1992). The design of joints between elastically dissimilar components (with special reference to ceramic/metal joints). *J. Strain Analysis* **27,** 15–20.

Li, F. Z., Shih, C. F. and Needleman, A. (1985). A comparison of methods for calculating energy release rates. *Engng Fract. Mech.* **21,** 405–421.

Matos, P. P. L., McMeeking, R. M., Charalambides, P. G. and Drory, M. D. (1989). A method for calculating stress intensities in bi-material fracture. *Int. J. Fract.* **40,** 235–254.

Muskhelishvili, V. I. (1953). *Some Basic Problems of the Mathematical Theory of Elasticity*, P. Noordoof and Company, NY.

Parks, D. M. (1974). A stiffness derivative finite element technique for determination of crack tip stress intensity factors. *Int. J. Fract.* **10,** 487–501.

Reedy Jr., E. D. (1990). Intensity of the stress singularity at the interface-corner between a bonded elastic and rigid layer. *Engng Fract. Mech.* **36,** 575–583.

Reedy Jr., E. D. (1993). Asymptotic interface-corner solutions for butt tensile joints. *Int. J. Solids Struct.* **30,** 767–777.

Rice, J. R. (1988). Elastic fracture mechanics concepts for interfacial cracks. *J. Appl. Mech.* **55,** 98–103.

Sham, T. L. (1991). The determination of elastic T-term using higher order weight functions. *Int. J. Fract.* **48,** 81–102.

Sinclair, G. B., Okajima, M. and Griffin, J. H. (1984). Path independent integral for computing stress intensity factors at sharp notches in elastic strips. *Int. J. Num. Methods Engng* **20,** 999–1008.

Sokolnikoff, I. S. (1956). *Mathematical Theory of Elasticity*, 2nd edition, McGraw Hill, NY.

Stern, M., Becker, E. D. and Dunham, R. S. (1976). A contour integral computation of mixed mode stress intensity factors. *Int. J. Fract.* **12,** 359–368.

Suga, T., Elssner, G. and Schmander, S. (1988). Composite parameters and mechanical compatibility. *J. Comp. Mat.* **22,** 917–935.

Theocaris, P. S. (1974). The order of singularity at a multi-wedge corner in a composite strip. *Int. J. Engng Sci.* **12,** 102–120.

van Vroonhoven, J. C. W. (1992). Stress singularity in bimaterial wedges with adhesion and delamination. *Fatigue Fract. Engng Mat. Struct.* **15,** 159–171.

Williams, M. L. (1952). Stress singularities resulting from various boundary conditions in angular corners of strips in extension. *J. Appl. Mech.* **74,** 526–528.

APPENDIX A

The eigen problem

In this appendix we derive the free-edge singular stress and displacement fields for the bi-material geometry shown in Fig. 2a. Consider a bi-material strip of width w and length $2L$ ($L \gg w$), subjected to a uniform remote tensile stress σ, as shown in Fig. 2a. We assume that the two materials are perfectly bonded at the interface and that plane strain conditions apply. The corner geometry is such that the traction-free surface of both materials make an angle of $\pi/2$ with the interface. The point where the interface meets the traction-free surface is referred to as the interface-corner; this point is denoted by A in Fig. 2a. The materials above and below the interface are referred to as materials 1 and 2, respectively. The two Dundurs (1969) elastic mismatch parameters α and β which govern the plane strain deformation of the bi-material are defined by (1). Let (x, y) and (r, θ) be rectangular and cylindrical polar co-ordinates centred at the interface-corner as shown in Fig. 2a. We describe below a procedure to determine the singular stress and displacement fields near the interface-corner A.

For the geometry shown in Fig. 2a, the stresses and displacements in material m ($m = 1, 2$) around the interface corner in the absence of body forces can be expressed in terms of two complex potentials Φ_m and Ω_m by (Muskhelishvili, 1953)

$$\sigma_y^m - i\sigma_{xy}^m = \bar{\Phi}_m'(\bar{z}) + \Phi_m'(z) + z\bar{\Phi}_m''(\bar{z}) + \bar{\Omega}_m'(\bar{z})$$

$$\sigma_x^m + i\sigma_{xy}^m = \bar{\Phi}_m'(\bar{z}) + \Phi_m'(z) - z\bar{\Phi}_m''(\bar{z}) - \bar{\Omega}_m'(\bar{z})$$

$$u_x^m + iu_y^m = (2\mu_m)^{-1}[\kappa_m \Phi(z) - z\bar{\Phi}_m'(\bar{z}) - \bar{\Omega}_m(\bar{z})]. \tag{A1}$$

Here, $z = x+iy = re^{i\theta}$ ($i^2 = -1$; $e^{i\theta} = \cos\theta + i\sin\theta$) is the complex co-ordinate, μ_m is the shear modulus, $\kappa_m \equiv 3-4\nu_m$ for plane strain and ν_m is Poisson's ratio for material m. The overbar denotes the complex conjugate and the ($'$) denote differentiation with respect to z. The stresses and displacements in polar co-ordinates are obtained from (A1) by transformation as

$$\sigma_{\theta\theta}^m - i\sigma_{r\theta}^m = \bar{\Phi}_m'(\bar{z}) + \Phi_m'(z) + \bar{z}\bar{\Phi}_m''(\bar{z}) + z^{-1}\bar{z}\bar{\Omega}_m'(\bar{z})$$

$$\sigma_r^m + i\sigma_{r\theta}^m = \bar{\Phi}_m'(\bar{z}) + \Phi_m'(z) - \bar{z}\bar{\Phi}_m''(\bar{z}) - z^{-1}\bar{z}\bar{\Omega}_m'(\bar{z})$$

$$u_r^m + iu_\theta^m = (2\mu_m)^{-1} e^{-i\theta}[\kappa_m\Phi(z) - z\bar{\Phi}_m'(\bar{z}) - \bar{\Omega}_m(\bar{z})]. \tag{A2}$$

Following England (1971), Stern *et al.* (1976) and Carpenter and Byers (1987), we assume the complex functions have the following asymptotic form as $z \to 0$,

$$\Phi_1 = Az^\lambda, \quad \Omega_1 = Bz^\lambda \quad \text{for material 1}$$

$$\Phi_2 = Cz^\lambda, \quad \Omega_2 = Dz^\lambda \quad \text{for material 2} \tag{A3}$$

where $A(=A_1+iA_2)$, $B(=B_1+iB_2)$, $C(=C_1+iC_2)$ and $D(=D_1+iD_2)$ are assumed to be complex constants. Bogy (1971) and Kelly *et al.* (1992) have shown that λ is real for the free-edge geometry shown in Fig. 2a.

We seek the free-edge stress and displacement fields that satisfy the following boundary conditions:

$$\sigma_{\theta\theta}^1 - i\sigma_{r\theta}^1 = \sigma_{\theta\theta}^2 - i\sigma_{r\theta}^2 \quad \text{along } \theta = 0$$

$$u_r^1 + iu_\theta^1 = u_r^2 + iu_\theta^2 \quad \text{along } \theta = 0$$

$$\sigma_{\theta\theta}^1 - i\sigma_{r\theta}^1 = 0 \quad \text{along } \theta = \pi/2$$

$$\sigma_{\theta\theta}^2 - i\sigma_{r\theta}^2 = 0 \quad \text{along } \theta = -\pi/2 \tag{A4}$$

where superscripts 1 and 2 denote the material index. Substitution of (A3) and (A4) into (A2) gives

$$A + \lambda\bar{A} + \bar{B} - C - \lambda\bar{C} - \bar{D} = 0 \tag{A5}$$

$$\kappa_1 A - \lambda\bar{A} - \bar{B} - \mu(\kappa_2 C - \lambda\bar{C} - \bar{D}) = 0 \tag{A6}$$

$$e^{i\lambda\pi/2}A - e^{i\lambda\pi/2}\lambda\bar{A} + e^{-i\lambda\pi/2}\bar{B} = 0 \tag{A7}$$

$$e^{-i\lambda\pi/2}C - e^{i\lambda\pi/2}\lambda\bar{C} + e^{i\lambda\pi/2}\bar{D} = 0 \tag{A8}$$

where $\mu = \mu_1/\mu_2$.

By considering the real and imaginary parts of eqns (A5)–(A8), we obtain eight homogeneous linear equations in the eight unknown coefficients A_m, B_m, C_m, D_m ($m = 1, 2$). A non-trivial solution to the equations exist only if the determinant of the coefficient matrix vanishes. This occurs when the eigenvalue λ satisfies the characteristic equation

$$16(\mu-1)^2[\lambda^2 - \sin^2(\lambda\pi/2)]^2 - 4[\mu(\kappa_2+1) - (\kappa_1+1)]^2[\lambda^2 - \sin^4(\lambda\pi/2)]$$

$$+ 16(\mu-1)\sin^2(\lambda\pi/2)[\mu(\kappa_2+1) - (\kappa_1+1)][\lambda^2 - \sin^2(\lambda\pi/2)] + [\mu(\kappa_2+1) + (\kappa_1+1)]^2\sin^2(\lambda\pi) = 0. \tag{A9}$$

We seek the smallest value of λ in the interval $0 < \lambda \leqslant 1$ as the solution to the characteristic eqn (A9). The roots of (A9) with $0 < \lambda \leqslant 1$ give unbounded stresses and vanishing displacements as the interface-corner is approached.

Bogy (1971) has previously determined the order of the singularity for two bonded elastic wedges of different materials and obtained a characteristic equation that is equivalent to (A9) when the wedge angles are identical to those of Fig. 2a; i.e., $\theta_1 = \theta_2 = \pi/2$. The value of λ is obtained by solving (A9) numerically for various values of material elastic mismatch parameters α and β; the results are plotted in Fig. A1 for all possible α and for $\beta = 0$

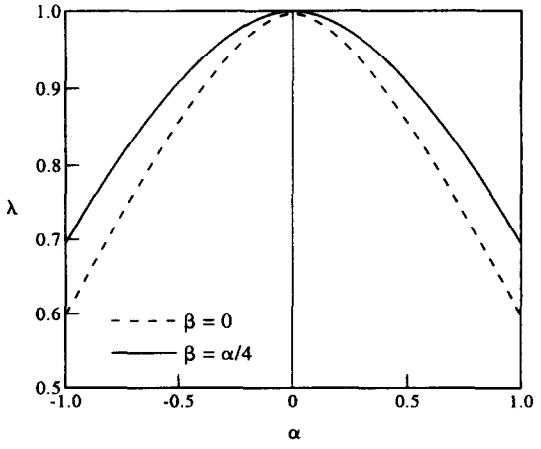

Fig. A1. The order of the displacement singularity λ at the free-edge for the uncracked bi-material geometry shown in Fig. 2(a).

and $\beta = \alpha/4$. In the limit $\alpha = \beta = 0$ the only possible solutions to (A9) are integer values of λ: no singularity exists at the interface-corner for $\alpha = \beta = 0$ as expected. Further, there is no stress singularity at the interface-corner of the geometry shown in Fig. 2a (i.e., $\lambda = 1$) for material combinations with $\beta = \alpha/2$ (see Bogy (1971) and Kelly *et al.* (1992)). We note that $\lambda(\alpha, \beta) = \lambda(-\alpha, -\beta)$, and that if λ is an eigenvalue for a given (α, β) pair, then so is $-\lambda$ for the same value of (α, β).

Once the value of λ has been obtained from eqn (A9), we can express seven of the eight unknown constants in terms of the eighth, say A_1, by substituting the value of λ into eqns (A5)–(A8). The unknown constant A_1 is normalised such that

$$\sigma_{\theta\theta}(\theta = 0) = Hr^{\lambda - 1}. \tag{A10}$$

By solving for the coefficients $A_2, B_1, \ldots, D_2$ in eqns (A5)–(A8) for known value of λ in terms of A_1, and applying the definition (A10), it can be shown that H is related to the coefficients $A_1, A_2, \ldots, D_2$ by

$$\begin{Bmatrix} A_1 \\ A_2 \\ B_1 \\ B_2 \\ C_1 \\ C_2 \\ D_1 \\ D_2 \end{Bmatrix} = \begin{bmatrix} 1 & 0 \\ 0 & 1 \\ x_{31} & x_{32} \\ x_{41} & x_{42} \\ x_{51} & x_{52} \\ x_{61} & x_{62} \\ x_{71} & x_{72} \\ x_{81} & x_{82} \end{bmatrix} \begin{Bmatrix} y_1 \\ y_2 \end{Bmatrix} H \tag{A11a}$$

or

$$\begin{Bmatrix} \mathbf{Q1} \\ \mathbf{Q2} \end{Bmatrix} = \begin{bmatrix} \underset{4\times 2}{\mathbf{X1}} \\ \underset{4\times 2}{\mathbf{X2}} \end{bmatrix} \{\underset{2\times 1}{\mathbf{Y}}\} H \tag{A11b}$$

where

$$\{\mathbf{Q1}\} = \{A_1 \quad A_2 \quad B_1 \quad B_2\}^{\mathrm{T}}$$
$$\{\mathbf{Q2}\} = \{C_1 \quad C_2 \quad D_1 \quad D_2\}^{\mathrm{T}} \tag{A12}$$

and

$$x_{31} = \lambda - \cos\lambda\pi$$

$$x_{32} = \sin\lambda\pi$$

$$x_{41} = \sin\lambda\pi$$

$$x_{42} = \lambda + \cos\lambda\pi$$

$$x_{51} = \frac{2(\mu-1)(\lambda + \sin^2(\lambda\pi/2)) + \kappa_1 + 1}{\mu(1+\kappa_2)}$$

$$x_{52} = \frac{(\mu-1)\sin\lambda\pi}{\mu(1+\kappa_2)}$$

$$x_{61} = -\frac{(\mu-1)\sin\lambda\pi}{\mu(1+\kappa_2)}$$

$$x_{62} = \frac{2(\mu-1)(\sin^2(\lambda\pi/2) - \lambda) + \kappa_1 + 1}{\mu(1+\kappa_2)}$$

$$x_{71} = \frac{[2(\mu-1)(\lambda + \sin^2(\lambda\pi/2)) + (\kappa_1+1)](\lambda - \cos\lambda\pi) + (\mu-1)\sin^2(\lambda\pi)}{\mu(1+\kappa_2)}$$

$$x_{72} = \frac{[3\lambda(\mu-1) - \kappa_1 - \mu]\sin\lambda\pi}{\mu(1+\kappa_2)}$$

$$x_{81} = -\frac{[3\lambda(\mu-1) + \kappa_1 + \mu]\sin\lambda\pi}{\mu(1+\kappa_2)}$$

$$x_{82} = \frac{[2(\mu-1)(\sin^2(\lambda\pi/2) + \lambda) + (\kappa_1+1)](\lambda + \cos\lambda\pi) - (\mu-1)\sin^2(\lambda\pi)}{\mu(1+\kappa_2)}$$

$$y_1 = \frac{[\mu(\kappa_2+1) + (\kappa_1+1)] - 4\lambda(\mu-1)}{4\lambda[(1+\kappa_1)(\lambda + \sin^2(\lambda\pi/2)) - (\mu-1)(\lambda^2 + \sin^2(\lambda\pi/2))]}$$

$$y_2 = \frac{2(\mu-1)(\lambda^2+2\lambda\sin^2(\lambda\pi/2)+\sin^2(\lambda\pi/2))-[\mu(\kappa_2+1)-(\kappa_1+1)](\lambda+\sin^2(\lambda\pi/2))}{2\lambda\sin(\lambda\pi)[(1+\kappa_1)(\lambda+\sin^2(\lambda\pi/2))-(\mu-1)(\lambda^2+\sin^2(\lambda\pi/2))]}. \tag{A13}$$

In the above equations, the superscript T denotes the transpose.

The stresses and displacements in the region dominated by the singularity can now be determined in terms of the unknown free-edge intensity factor, H, by substituting eqns (A3) and (A11) into eqn (A2). The stresses and the displacements, which are the eigenfunctions corresponding to the eigenvalue λ, are given by

$$\sigma_{ij}^m = Hr^{\lambda-1} f_{ij}^m(\lambda,\theta)$$
$$u_i^m = Hr^{\lambda} g_i^m(\lambda,\theta) \tag{A14}$$

where $m(=1,2)$ denotes the material number, $(i,j) \equiv (r,\theta)$ represents the cylindrical polar co-ordinates centred at the interface-corner, and the functions f_{ij} and g_i are defined below.

Define a matrix $\{\mathbf{F}\}$ by

$$\{\mathbf{F}\} = [g_r^1 \quad g_\theta^1 \quad f_{rr}^1 \quad f_{\theta\theta}^1 \quad f_{r\theta}^1 \quad g_r^2 \quad g_\theta^2 \quad f_{rr}^2 \quad f_{\theta\theta}^2 \quad f_{r\theta}^2]^{\mathrm{T}} \tag{A15}$$

where the superscripts 1 and 2 again denote the material indices. Then,

$$\{\mathbf{F}\} = \begin{bmatrix} \underset{5\times4}{\mathbf{N}} & 0 \\ 0 & \underset{5\times4}{\mathbf{M}} \end{bmatrix} \begin{Bmatrix} \underset{4\times2}{\mathbf{X1}} \\ \underset{4\times2}{\mathbf{X2}} \end{Bmatrix} \begin{Bmatrix} \mathbf{Y} \\ {}_{2\times1} \end{Bmatrix} \tag{A16}$$

where

$$[\mathbf{N}] = \begin{bmatrix} \dfrac{(\kappa_1-\lambda)\cos(\lambda-1)\theta}{2\mu_1} & \dfrac{(\lambda-\kappa_1)\sin(\lambda-1)\theta}{2\mu_1} & -\dfrac{\cos(\lambda+1)\theta}{2\mu_1} & \dfrac{\sin(\lambda+1)\theta}{2\mu_1} \\ \dfrac{(\kappa_1+\lambda)\sin(\lambda-1)\theta}{2\mu_1} & \dfrac{(\kappa_1+\lambda)\cos(\lambda-1)\theta}{2\mu_1} & \dfrac{\sin(\lambda+1)\theta}{2\mu_1} & \dfrac{\cos(\lambda+1)\theta}{2\mu_1} \\ \lambda(3-\lambda)\cos(\lambda-1)\theta & \lambda(\lambda-3)\sin(\lambda-1)\theta & -\lambda\cos(\lambda+1)\theta & \lambda\sin(\lambda+1)\theta \\ \lambda(\lambda+1)\cos(\lambda-1)\theta & \lambda(\lambda+1)\sin(1-\lambda)\theta & \lambda\cos(\lambda+1)\theta & -\lambda\sin(\lambda+1)\theta \\ \lambda(\lambda-1)\sin(\lambda-1)\theta & \lambda(\lambda-1)\cos(\lambda-1)\theta & \lambda\sin(\lambda+1)\theta & \lambda\cos(\lambda+1)\theta \end{bmatrix}. \tag{A17}$$

The matrix $[\mathbf{M}]$ is obtained by replacing κ_1 by κ_2 and μ_1 by μ_2 in the definition of $[\mathbf{N}]$. The unknown parameter H is determined for the specific geometry and applied loading as described below in Appendix B.

APPENDIX B

Integral contour method for evaluating the free-edge intensity factor H

In this appendix we describe the method used to evaluate the free-edge intensity factor H for the bi-material geometry shown in Fig. 2a. The bi-material strip is subjected to a remote stress σ, and the stress-free surfaces of both materials intersect the interface at an angle of $\pi/2$ at the interface-corner A (see Fig. 2a). Let (r,θ) be polar co-ordinates centred at the interface-corner A. We assume that plane strain conditions apply, and describe below the procedure to evaluate the intensity H of the singularity that develops near the interface-corner A due to the remote load σ.

The stress and displacement fields around the interface-corner in material m ($m = 1,2$) are given by (A14). The free-edge intensity factory H is determined by the reciprocal work integral contour method. This method has been used by various authors to obtain the stress intensities for different crack and notch geometries; see, for example, Stern *et al.* (1976), Sinclair *et al.* (1985), and Carpenter and Byers (1987). The reciprocal work integral contour method is based on the reciprocal theorem (Sokolnikoff, 1956).

Consider a closed contour $C(=C_1+C_2+C_3+C_4)$ around the interface-corner, as shown in Fig. 3. The reciprocal theorem can be stated as

$$\oint_C (\sigma_{ij}u_i^* - \sigma_{ij}^* u_i) n_j \, \mathrm{d}s = 0 \tag{B1}$$

where $(i,j) \equiv (r,\theta)$ represent the polar co-ordinates centred at the interface-corner, σ_{ij} and u_i are the free-edge singular stress and displacement fields given by eqn (A14), σ_{ij}^*, u_i^* are auxiliary fields satisfying the same field equations as σ_{ij} and u_i (i.e., eqn (A4)), n_j are the components of a unit outward normal to C, and $\mathrm{d}s$ is an infinitesimal line segment of C. The integration in (B1) is performed in an anticlockwise sense around C. By suitable choice of the auxiliary field (σ_{ij}^*, u_i^*), the evaluation of the integral (B1) can be used to determine the free-edge intensity factor H.

To proceed we consider the auxiliary field

Table B1. Tabulated solutions for the integral h as a function of material mismatch parameters α and β

	$\alpha = 0$	$\alpha = 0.2$	$\alpha = 0.5$	$\alpha = 0.8$	$\alpha = 0.99$
$\beta = 0$	−573.5962	−0.1401	−0.0809	−0.1759	−3.6819
$\beta = \alpha/4$	−573.5962	−0.2391	−0.0882	−0.1380	−2.4871

Note that $h(-\alpha, -\beta) = h(\alpha, \beta)$.

$$\sigma_{ij}^{*m} = H^* r^{\lambda^*-1} f_{ij}^{*m}(\lambda^*, \theta)$$
$$u_i^{*m} = H^* r^{\lambda^*} g_i^{*m}(\lambda^*, \theta) \tag{B2}$$

where $m(=1, 2)$ denotes the material index,

$$\lambda^* = -\lambda$$
$$f_{ij}^{*m}(\lambda^*, \theta) = f_{ij}^{m}(-\lambda, \theta)$$
$$g_i^{*m}(\lambda^*, \theta) = g_i^{m}(-\lambda, \theta) \tag{B3a}$$

and

$$\sigma_{\theta\theta}^{*1} = \sigma_{\theta\theta}^{*2} = H^* r^{\lambda^*-1} \quad (\text{along } \theta = 0). \tag{B3b}$$

H^* is the intensity of the auxiliary field.

As discussed in Appendix A, if λ is an eigenvalue for a given pair of materials such that the eigenvectors (stresses and displacements) satisfy the field equations (A4), then $\lambda^* = -\lambda$ is also an eigenvalue for the same material pair. As portions C_1 and C_3 of the closed contour C are traction-free (see Fig. 3),

$$\sigma_{ij}^* n_j = \sigma_{ij} n_j = 0 \tag{B4}$$

on these surfaces. Therefore eqn (B1) becomes

$$\int_{C_4} (\sigma_{ij} u_i^* - \sigma_{ij}^* u_i) n_j \, ds = -\int_{C_2} (\sigma_{ij} u_i^* - \sigma_{ij}^* u_i) n_j \, ds. \tag{B5}$$

The integral on the left hand side of eqn (B5) (i.e., along C_4) is evaluated by substituting the asymptotic field eqn (A14) for the unstarred field (σ_{ij}, u_i), and the asymptotic field given by eqn (B2) for the auxiliary starred field (σ_{ij}^*, u_i^*). Thus, we have

$$I = \int_{C_4} (\sigma_{ij} u_i^* - \sigma_{ij}^* u_i) n_j \, ds \equiv hHH^* \tag{B6}$$

where

$$h = \int_{C_4} [f_{ij}(\lambda, \theta) g_i(-\lambda, \theta) - f_{ij}(-\lambda, \theta) g_i(\lambda, \theta)] \, d\theta. \tag{B7}$$

The functions f_{ij} and g_i are defined in Appendix A. Integration of (B7) is performed numerically to obtain the value of h. In the evaluation of h, the contour C_4 is divided into 40 equal angular segments and the integration is performed using a ten point Gaussian quadrature integration formula within each segment; the numerically obtained values of h are given in Table B1.

Integration of the right hand side of eqn (B5) along C_2 is performed by the domain integration method (see Li *et al.* (1985)), whereby the line integral is converted to an area integral via Gauss's theorem. For evaluation of the integral along C_2, the stresses and displacements (σ_{ij}, u_i) are obtained by the finite element method at the integration points of all the elements within a chosen domain of integration. However, the stresses and the displacements for the auxiliary field (σ_{ij}^*, u_i^*) at the integration points of these elements are determined from eqn (B2). The intensity of the auxiliary field H^* is chosen as $H^* = 1/h$, where h is given by (B7). Thus, from eqns (B5) and (B6), the value of the integration along C_2 becomes

$$H = -\int_{C_2} (\sigma_{ij} u_i^* - \sigma_{ij}^* u_i) n_j \, ds. \tag{B8}$$

Once H has been determined using the above procedure, the value of the non-dimensional constant $a(\alpha, \beta)$ is obtained via eqn (4). The calculated values of the non-dimensional constant $a(\alpha, \beta)$ are independent of the path chosen for the integration. For example, values for $a(0.8, 0.2)$ differ by less than 0.01% for eight different domains of integration, with inner radius ranging from $r = 0.003w$ to $r = 0.004w$ and outer radius ranging from $r = 0.06w$ to $r = 0.065w$.